LAWRENCE
LIVERMORE
NATIONAL
LABORATORY

UCRL-JRNL-205764

Analytic Model of Reactive Flow

P. Clark Souers, Peter Vitello

August 5, 2004

Propellants, Explosives, Pyrotechnics

UCRL-JRNL-205764 August 6, 2004 to *Propellants, Explosives, Pyrotechnics*

Analytic Model of Reactive Flow

P. Clark Souers and Peter Vitello
Energetic Materials Center, Lawrence Livermore National Laboratory, Livermore, CA USA 94550

Abstract

A simple analytic model allows prediction of rate constants and size effect behavior before a hydrocode run. It is applied to near-ideal PBX 9404, in-between ANFO and most non-ideal AN. The power of the pressure declines from 2.3, 1.5 to 0.8 across this set. The power of the burn fraction, F, is 0.8, 0 and 0, so that an F-term is important only for the ideal explosives. The (1-F) term has a power of 1.5, 1 and 1. The size effect shapes change from concave-down to nearly straight to concave-up. Failure occurs for ideal explosives when the calculated detonation velocity turns in a double-valued way. The effect of the power of the pressure may be simulated by including a pressure cutoff in the detonation rate.

Keywords: model, reactive flow, detonation rate, rate constant, size effect

1 Introduction

Reactive Flow is the class of explosive models where the chemistry of detonation is simulated by an overall reaction rate and where the rate constant is assumed to be truly constant. The first test of this model is to calculate the size (diameter) effect, which is a plot of detonation velocity versus inverse radius of a cylindrical explosive part.

A wide spectrum of explosives may be indicated by considering three general classes, which must all fitted. 1) The nearly straight line in the size effect plot is shown by ammonium nitrate emulsion k1a and ANFO prill which fail with a radius of 6-10 mm and a detonation velocity ratio U_S/D of about 0.6. **[1-3]** 2) The more nearly ideal PBX 9404 and Comp B have a shape that is strongly concave down in inverse radius space. The explosives fail at 0.6 – 2 mm, which amounts to a ratio, U_S/D, of about 0.83-0.85. **[4,5]** These explosives do not decrease much in detonation velocity before they fail. 3) The more non-ideal ammonium nitrate at 1.0 g/cm^3 and Australian heavy ammonium nitrate emulsion. HANFO, are concave-up in shape, fail at 25-70 mm with a U_S/D of 0.25-0.31. **[6,7]**

In the simple reactive flow code JWL++, these three have usually had detonation rates with powers of the pressure equal to 1, 2-3, and 1, respectively. **[8]**

To model size effect behavior, Leiper, Kirby and Cooper suggested a Gaussian function that modulates the energy delivery over the range of the burn fraction, F. **[9-11]** In their 1-D, three-rate model, they reproduced the concave-up size effect shape of AN slurry and nitrogylcerine powder using a Gaussian

function peaked at the early burn fraction of 0.15. They also reproduced the concave-down shape of Comp B with a late energy delivery peak at a burn fraction of 0.7. Their Gaussian functions did not run continuously from 0 < F < 1 but turned on at some initial value of F. The rate was proportional to pressure to the first power. This approach states that energy delivery early or late in the reaction zone can affect the size effect curve. This leads to the idea used here that the burn fraction may be linked to detonation velocity in a continuous way for all radii of a given explosive.

2 Necessary Input Relations

We here suggest a simple 1-D model that can be run prior to hydrocodes to estimate possible reactive flow behavior. We need a set of approximate relations, starting with the Eyring equation **[12]**

$$U_S = D\left(1 - \frac{< x_e >}{\sigma R_o}\right) \tag{1}$$

where U_s and D are the detonation velocities at radius R_o and infinite radius, $<x_e>$ is the average reaction zone length derived from edge lag measurements by using σ which is given by **[13]**

$$\sigma = 0.4\left(1 - (U_S / D)^2\right)^{-0.8}. \tag{2}$$

Also, the time to cross the reaction zone, t_e, is given by

$$t_e = \frac{< x_e >}{U_S}. \tag{3}$$

The most important relation is

$$F_e \approx \left(U_S / D\right)^2 \approx P_m / P_m^o. \tag{4}$$

where F_e is the burn fraction and P_m and $P_m{}^o$ are the maximum pressures at radius R_o and infinite radius. The maximum pressure is the spike at about 1.5 times the C-J pressure. Eq. (4) is so important its derivation is given in detail in the Appendix. It is approximate but very useful.

3 The Simple Model

The rate equation for a one rate model is

$$\frac{dF}{dt} = G_1 P^b F^a (1-F)^c \tag{5}$$

where G_1 is the rate constant. We collect F on the left and integrate to F_e to get the result

$$I = \int_0^{F_e} \frac{dF}{F^a (1-F)^c} \approx G_1 \left(P_m^o F_e \right)^b t_e . \tag{6}$$

In the reaction zone, the pressure declines from P_m to C-J, but we shall use a constant pressure for simplicity. We substitute Eqs. (1) –(4) to get

$$I = R_o \left(\frac{G_1}{D} \left(P_m^o \right)^b \right) \sigma \left(F_e^{b-1/2} (1 - F_e^{1/2}) \right). \tag{7}$$

We define a dimensionless radius

$$R_D = \frac{D}{G_1^o (P_m^o)^b} \tag{8}$$

where the rate constant is now made a true constant $G_1{}^o$ derived from size effect data as described below. We rearrange to get

$$\frac{R_D}{R_o} = \frac{\sigma}{I} \left(F_e^{b-1/2} (1 - F_e^{1/2}) \right) . \tag{9}$$

Eq. (9) will be solved for R_D/R_o, which we plot versus U_s/D in a generalized size effect plot.

4 Estimating G_1^o

How do we estimate the constant G_1^o from real data? The average detonation rate is inversely proportional to the slope of the size effect curve. **[8]** This effect is easily seen in the codes by changing rates and watching the curves rotate about the infinite-radius detonation velocity, D. We take Eq. (5) and convert it to average values

$$\left\langle \frac{dF}{dt} \right\rangle \approx \frac{-DU_s}{\partial U_s / \partial (1/R_o)} \approx G_1 \left(P_m^o < F_e > \right)^b < F >^a < 1-F >^c . \tag{10}$$

where <dF/dt> in μs^{-1} is independent of models. The average value <F> is set to be 1/2. We next move to infinite radius, where $F_e = 1$, so that term disappears. The measured rate $<dF/dt>_o$ is obtained by extrapolating the detonation rate versus inverse radius to infinite radius, which is the same procedure used to get D. Then, G_1 becomes G_1^o, which is expected to be constant for all radii. We have a problem with the averages of F. First, we are not sure what value to use if evaluated at infinite radius. Second, they are a function of a and c, which is extremely inconvenient in repetitive calculating and plotting. We shall try an intermediate position, where use the a = 0, c = 1 value of 1/2 everywhere. We then get at infinite radius

$$G_1^o \approx \frac{2}{\left(P_m^o \right)^b} \left\langle \frac{dF}{dt} \right\rangle_o = constant . \tag{11}$$

We see that $G_1^o (P_m^o)^b$ and R_D are indeed constant with respect to b, which is an important relation. This produces the effect where if b increases, so does G_1^o. We get the generalized radius

$$R_D \approx \frac{D}{2 < dF / dt >_o} \tag{12}$$

which is what we shall use to plot the data.

5 Results

The straight-line type of explosives are shown in Figure 1: AN emulsion k1a and ANFO prill. These are easily fit with a = 0, c = 1 and b = 1.5.

The near-ideal, concave-down explosive PBX 9404 is shown in Figure 2. The bend is so great that the entire curve lies in a small R_D/R_o range. To get this effect, we need a large value of a = 0.67 and of b = 2.3, and this is shown by the heavy line.

Figure 3 goes to other extreme at large R_D/R_o values with the ultra-slow, super non-ideal explosives 1.0 g/cc AN, potassium chlorate 80/sugar **[14]** and HANFO (Australian heavy AN emulsion). We use a = 0, c = 1, b = 0.8 to get a concave-up shape.

We have fit all three kinds of explosives by increasing b_1 going from non-ideal to ideal and by inserting an F^a term for ideal explosives only.

6. Pressure Cutoff

Leiper, et. al. made an analytical 1-D model that used b = 1 with a pressure cutoff P_o to create the concave-down shape as well as failure. **[9-11]** For $P < P_o$, $G_1 = 0$. This can be added to give

$$R_D = \frac{D}{G_1^o (P_m^o - P_o)^b} \tag{13}$$

with everything else the same. The result is shown by the fine line in Figure 2, where the concave-down shape is given with b = 1 combined with $P_o/P_m{}^o = 0.3$. A large value of a is still needed.

The effect of a large b or pressure cutoff is to create a double valued curve, where the turn (with zero rate from Eq. (10)) may be taken as failure of the detonation. This applies only in the region of small R_D/R_o. At large R_D/R_o, failure occurs by the merging of the detonation with the undetonated explosive at low U_s/D values. In between, we have no mechanism for failure.

Appendix

A1 Energy-Detonation Velocity Relation

In one slice of ideal detonating explosive, let a fraction 2α of the detonation energy E_o be released to move forward to be the energy of compression, E_c, for the next slice so that

$$\begin{aligned} E_C &= \alpha E_O \\ E_S &= (1+\alpha)E_O \end{aligned}. \tag{A-1}$$

There, the energy PdV is deposited. Half of it compresses the explosive and half goes to accelerate the mass and the other half goes into internal energy. The energy of compression is

$$E_C = \frac{1}{2}P(1-v) = \frac{1}{2}\rho_O u_p^2. \tag{A-2}$$

We move to the internal energy side. The sound speed is given by

$$c^2 = -\frac{v^2}{\rho_O}\frac{\partial P}{\partial v}. \tag{A-3}$$

We take the pressure from a crude JWL equation-of-state as being

$$P = A\exp(-Rv) \tag{A-4}$$

and we can relate the derivitive of P and the integral, E_s, of PdV by

$$\frac{\partial P}{\partial v} = -R^2 E_S. \tag{A-5}$$

The detonation velocity is the sum of the mass velocity and sound speed

$$U_S^2 = (u_p + c)^2 = \frac{1}{\rho_O}\left[\left(2E_C\right)^{1/2} + vRE_S^{1/2}\right]^2. \tag{A-6}$$

We subtitute Eq. (A-1) into Eq. (A-6) and divide by the infinite radius detonation velocity, D, to get

$$\frac{U_S}{D} = \left(\frac{E_O}{E_O^o}\right)^{1/2}\left[\frac{(2\alpha)^{1/2} + \nu R(1+\alpha)^{1/2}}{(2\alpha)^{1/2} + \nu_O R(1+\alpha)^{1/2}}\right] \approx F_e^{1/2}. \tag{A-7}$$

A2 Pressure-Detonation Velocity Relation

We substitute the approximate relation

$$u_p \approx \frac{U_S}{4} \tag{A-8}$$

into

$$P \approx \rho_O U_S u_p \tag{A-9}$$

to get

$$U_S \approx \left(\frac{4P}{\rho_O}\right)^{1/2}. \tag{A-10}$$

A combination of Eqs. (A-7) and (A-10) lead to the relation

$$\frac{P_m}{P_m^o} \approx F_e. \tag{A-11}$$

A3 Relations in the Model

We want to make an analytical model that simulates a reactive flow computer model and allows us to estimate the settings ahead of time. To start this, we need some relations for the same explosive at different radii, using $<E_o>$ and $<P_m>$ as averages across the entire detonation front. Because we have no real data to show the above relations, we turn to the reactive flow model JWL++ running in a 2-dimensional arbitrary Lagrangian-Eulerian (ALE) hydrocode with CALE-like properties. We shall run different radii of the same material. The sonic plane is found using the function

$$(u_{px}^2 + u_{py}^2)_i^{1/2} + C_i - U_s = 0. \tag{A-12}$$

where U_s is the detonation velocity in the ratestick found in the first code run and C is the speed of sound as determined by the equation-of-state. The particle velocities and sound speeds are in the ith zone on every cycle, so that their sum forms an instantaneous detonation velocity. When Eq. (A-12) equals zero, we are on the sonic plane, where no energy can move forward to the front. In a given zone, we plot the burn fraction versus the sonic function to get the burn fraction on the sonic plane. The maximum pressures are also obtained wherever they appear inside the reaction zone. The averages for the overall burn fraction and maximum pressure are given by

$$\langle F_e \rangle = \sum_i \lambda_i F_{ei}$$
$$\langle P_m \rangle = \sum_i \lambda_i P_{mi} \qquad \text{(A-13)}$$

.

where λ_i is the fraction of radial area. We need to use explosives that have large reaction zones and react at small burn fractions in order to get the resolution possible in mapping code output. The zoning is set so that we have a 35-50 zones radially and that the reaction zone contains 8 –12 zones. At least 12 slices and sometimes over 20 slices radially are taken in the analysis. For ratesticks 10 times longer than the radius, the results are constant at each radius and represent steady state conditions. The values of D and P_m come from extrapolation of the code results with the running of a large radius sample being essential to obtaining a good value.

The results are plotted in Figure A-1, The linear relations agree with the derivations we carried out.

Acknowledgements

This work was performed under the auspices of the U.S. Department of Energy by the University of California, Lawrence Livermore National Laboratory under Contract No. W-7405-Eng-48.

References

1. U. Nyberg, J. Deng and L. Chen, Matning av Detonationshastighet och Krokningsfront i Samband med Brinnmodellutveckling for Emulsionssprangamne K1, Swedish Rock Engineering Research, Stockholm, SveBeFo Report 6, **1995**.

2. J. Deng, S. Nie and L. Chen, *Determination of Burning Rate Parameters for an Emulsion Explosive*, Swedish Rock Engineering Research, Stockholm, SveBeFo Report 17, **1995**. Finn Ouchterlony kindly sent the Swedish Rock reports.

3. Richard Catanach, Los Alamos National Laboratory, Los Alamos, NM, private communications, **2002-2003**.

4. *LASL Explosive Property Data*, T. R. Gibbs and A. Popolato, ed., University of California Press, Berkeley, **1980**.

5. M. E. Malin, A. W. Campbell and G. W. Mautz, "Particle Size Effects in One- and Two-Component Explosives," *Second ONR Symposium on Detonation*, White Oak, MD, February 11, **1955**, pp. 478-493.

6. M. A. Cook, E. B. Mayfield and W. S. Partridge, Reaction Rates of Ammonium Nitrate in Detonation, *J. Phys. Chem.* **1955** *59*, 675-680.

7. David Kennedy, ICI Australia Operations, Kurri Kurri, New South Wales, Australia, private communications, **1995, 1997**.

8. P. Clark Souers, Steve Anderson, Estella McGuire, Michael J. Murphy, and Peter Vitello, Reactive Flow and the Size Effect, Propellants, *Explosives, Pyrotechnics* **2001**, *26*, 26-32.

9. I. J. Kirby and G. A. Leiper, A Small Divergent Detonation Theory for Intermolecular Explosives, *Proceedings Eighth Symposium (International) on Detonation*, Albuquerque, NM, July 15-19, **1985**, pp. 176-186.

10. G. A. Leiper and J. Cooper, Reaction Rates and the Charge Diameter Effect in Heterogeneous Explosives, *Proceedings Ninth Symposium (International) on Detonation*, Portland, OR, August 28- September 1, **1989**, pp. 197-207.

11. G. A. Leiper, Aberdeen, U. K., private communications, **2002-2003**.

12. H. Eyring, R. M. Powell, G. E. Duffey and R. B. Parlin, "The Stability of Detonation," *Chem Rev* **1949**, *45*, 144-146.

13. P. Clark Souers and Raul Garza, "Kinetic Information from Detonation Front Curvature." *Proceedings Eleventh International Detonation Symposium*, Snowmass Village , CO, August 30-September 4, **1998**, pp. 459-465.

14. Raul Garza and P. Clark Souers, Lawrence Livermore National Laboratory, private communication, **2003**.

Symbols and Abbreviations

A	JWL coefficient (GPa)
a	Pressure exponent for F (dimensionless)
b	Pressure exponent for pressure (dimensionless)
C	Speed of sound (mm/μs)
c	Pressure exponent for (1- F) (dimensionless)
D	Detonation velocity at infinite radius (mm/μs)
E_c	Compression energy (kJ/cm^3)
E_o	Detonation energy at radius R_o (kJ/cm^3)
E_o^o	Detonation energy at infinite radius (kJ/cm^3)
E_s	Internal energy (kJ/cm^3)
F	Burn fraction (dimensionless)

$\langle F \rangle$	Average burn fraction (dimensionless)
$\langle dF/dt \rangle$	Average detonation rate (μs^{-1})
$\langle dF/dt \rangle_o$	Average detonation rate at infinite radius (μs^{-1})
F_e	Burn fraction at the back of the reaction zone (dimensionless)
$\langle F_e \rangle$	Average burn fraction at the back of the reaction zone (dimensionless)
G_1	Rate constant ($\mu s GPa^{b1})^{-1}$
G_1^o	Rate constant at infinite radius ($\mu s GPa^{b1})^{-1}$
I	Integral of all F-terms (dimensionless)
i	Sub indicating ith zone (dimensionless)
P	Pressure (GPa)
P_m	Maximum pressure at radius R_o (GPa)
$\langle P_m \rangle$	Average maximum pressure at radius R_o (GPa)
P_m^o	Maximum pressure at infinite radius (GPa)
Q	Artificial viscosity (GPa)
R	Equation of state exponential coefficient (dimensionless)
R_D	Generalized radius (dimensionless)
R_o	Initial explosive radius (mm)
t	Time (μs)
t_e	Time at end of reaction zone (μs)
u_p	Particle velocity (mm/μs)
u_{px}	X-direction particle velocity (mm/μs)
u_{py}	Y-direction particle velocity (mm/μs)
U_s	Detonation velocity at radius R_o (mm/μs)
v	Relative volume of compression at radius R_o (dimensionless)
$\langle x_e \rangle$	Average reaction zone length (mm)
α	Coefficient linking compression and detonation energies (dimensionless)
λ	(dimensionless)
ρ_o	Initial explosive density (g/cm^3)
σ	Ratio skin layer thickness to reaction zone length

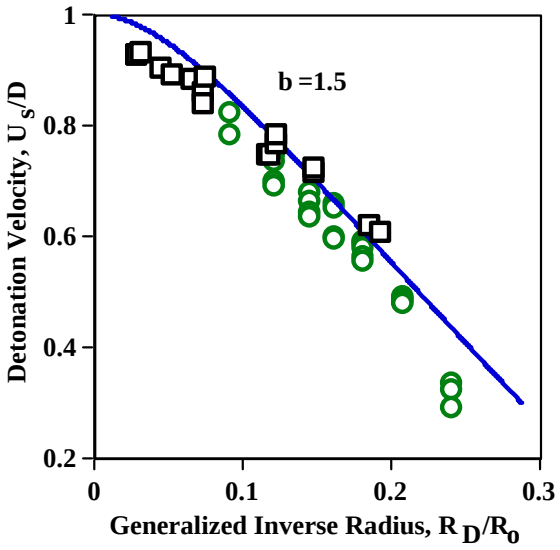

Figure 1. Near-straight line AN emulsion k1a (squares) and ANFO prill (circles) with b = 1.5 and a = 0, c = 1

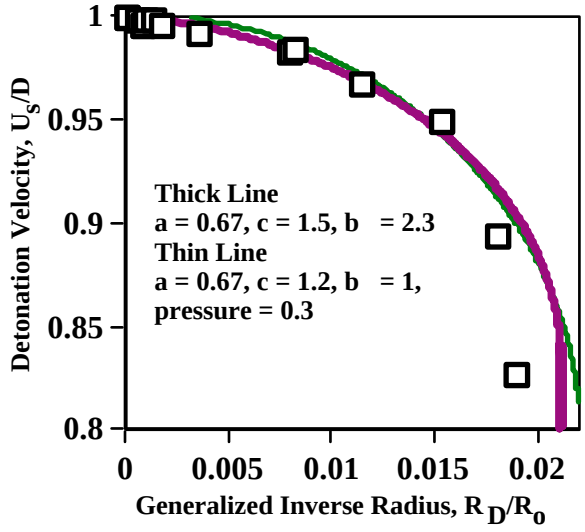

Figure 2. Extreme concave-down curve for PBX 9404. Usually, this takes a large a and b. Using a pressure cutoff reduces b but not a.

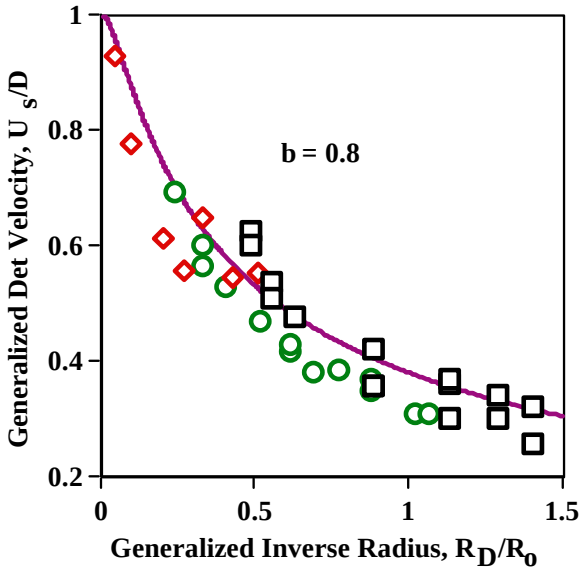

Figure 3. Concave-up shapes for AN (squares), potassium chlorate/sugar (diamonds) and HANFO (circles) with a = 0, c = 1 and b = 0.8.

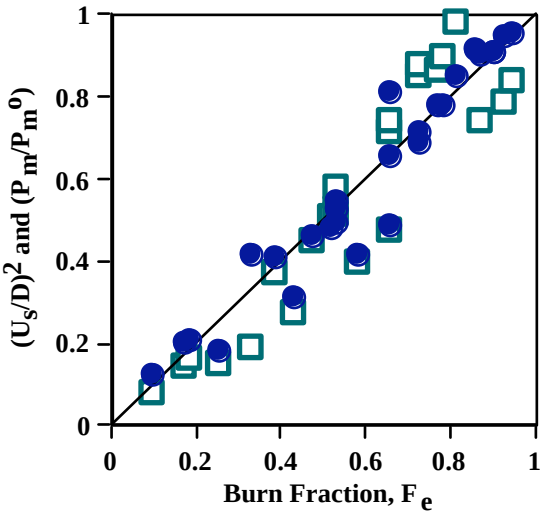

Figure A-1. Code plot of dimensionless detonation velocity-squared and pressure as a function of the burn fraction. The results are close to linear for both functions.